Organic Electronics 10 (2009) 594–606

Contents lists available at ScienceDirect

Organic Electronics

journal homepage: www.elsevier.com/locate/orgel

Highly branched green phosphorescent tris-cyclometalated iridium(III) complexes for solution-processed organic light-emitting diodes

Wei-Sheng Huang [a], Chia-Wei Lin [a], Jiann T. Lin [b,*], Jen-Hsien Huang [c], Chih-Wei Chu [c], Ying-Hsien Wu [d], Hong-Cheu Lin [a,*]

[a] Department of Materials Science and Engineering, National Chiao Tung University, Hsinchu, Taiwan, ROC
[b] Institute of Chemistry, Academia Sinica, Taipei, Taiwan, ROC
[c] Department of Chemical Engineering, National Taiwan University, Taipei, Taiwan, ROC
[d] Electro-optical Engineering and Graduate Institute of Electronics Engineering, National Taiwan University, Taipei, Taiwan, ROC

ARTICLE INFO

Article history:
Received 14 October 2008
Received in revised form 28 November 2008
Accepted 24 February 2009
Available online 3 March 2009

PACS:
78.60-Fi

Keywords:
Iridium complexes
Dendrimers
Phosphorescence
Organic light-emitting diodes

ABSTRACT

A series benzoimidazole-based dendritric complexes of iridium dendrimers containing Fréchet-type dendrons with peripheral fluorenyl surface groups have been synthesized. These iridium dendrimers are green-emitting with high phosphorescence quantum yield, and can be spin-coated as films of good quality. From cyclic voltammograms (CV), high onset potentials at 1.42–1.58 V due to the peripheral fluorene group were observed. Device from a second generation dendrimer **17** with structure of ITO/PEDOT:PSS/CBP: 20 wt% **17**/TPBI/LiF/Al (PEDOT:PSS = poly(ethylene dioxythiophene): polystyrenesulfonate and CBP = bis(*N*-carbazolyl)biphenyl) has the best performance: maximum external quantum efficiency of 13.58% and maximum current efficiency of 45.7 cd/A. Space-charge-limited current (SCLC) flow technique was used to measure the mobility of charge carriers in the blend films of the compounds in CBP. Blend films of higher generation dendrimers have lower hole mobility, albeit with higher device efficiencies.

1. Introduction

Since Tang and coworkers reported electroluminescent devices based on tris(8-hydroxyquinoline) aluminum (Alq_3) in 1987, organic light-emitting diodes (OLEDs) have attracted great attention [1]. In recent years, there are increasing numbers of solution-processed OLED devices fabricated from fluorescent polymers or dendrimers [2]. However, the devices exhibit only low efficiencies in most cases. A lot of efforts have been directed to phosphorescent materials in order to improve device efficiencies [3]. Because both singlet and triplet excitons can be harvested, theoretical 100% internal quantum efficiency is possible to be achieved in electrophosphorescent devices [4]. However, intermolecular interaction frequently leads to quenching of excited states and reduces the performance of OLEDs, fabricated via either vacuum deposition or solution-processing.

An ideal approach to suppress intermolecular interaction and retain high emission quantum yields is to use bulky and/or rigid peripheries to encapsulate the emitting core, i.e., dendritic approach [5,6]. Indeed, dendritic LEDs (DLEDs) using electrophosphorescent iridium dendrimers as emitters were reported to exhibit high luminous efficiency even without any host. For example, a maximum external quantum efficiency (EQE) of 13% and a maximum luminous efficiency of 34.7 cd A^{-1} were reported for green light-emitting iridium dendrimers with benzoimidazole-based ligands containing carbazolyl dendrons [7]. Similarly, a high EQE value of 13.6% (30 lm/W, 47 cd/A, 110 cd/m^2) was also achieved on a host-free DLED based on a dendrimer with a

* Corresponding authors. Fax: +886 2 27831237 (J.T. Lin); +886 3 5724727 (H.-C. Lin).
E-mail addresses: jtlin@chem.sinica.edu.tw (J.T. Lin), linhc@cc.nctu.edu.tw (H.-C. Lin).

1566-1199/$ - see front matter © 2009 Elsevier B.V. All rights reserved.
doi:10.1016/j.orgel.2009.02.022

fac-tris(2-phenylpyridyl)iridium(III) core [8]. Possibly due to the presence of void space and the insulating linkages inside a dendrimer, the carrier mobility generally decreases as the dendrimer generation increases [9]. Consequently, the dendrimers are commonly doped in host materials, such as bis(*N*-carbazolyl)biphenyl (CBP) [10], in order to improve the device efficiency. Red- [11], green- [7,12], and blue-emitting [13] DLEDs have been fabricated to demonstrate very promising efficiencies. It is worthy to note that besides encapsulation, dendrons surrounding the phosphorescent core also allow one to tether with suitable surface groups for enhancing the solubility of the dendrimer to facilitate spin-coating of the film [14], or tether with carrier-transport units for improving charge transporting [11,15].

Previously we synthesized a series of phosphorescent cyclometalated iridium complexes containing benzoimidazole-based ligands [16]. High performance DLEDs based on the complexes were fabricated via vacuum deposition. In a recent report we extended our study to Fréchet-type dendritic benzoimidazole ligands [17], and electroluminescent (EL) devices with good efficiencies can be achieved by solution-processing. In an attempt to further enlarge the size of Fréchet-type dendron, we tethered periphery with a fluorene moiety which was beneficial to raising the solubility and reducing the intermolecular interactions [12b]. Furthermore, fluorene moiety is also possible to assist in carrier hopping [18]. In this paper, we report the first- and second-generation cyclometalated iridium dendrimer, in which Fréchet-type benzyl ether-based dendrons were tethered with peripheral alkylated fluorenyl groups. DLEDs fabricated from these dendrimers by spin-coating technique will also be discussed.

2. Experimental

2.1. Characterization

The ^{1}H NMR spectra were recorded on a Bruker AMX400 spectrometer. FAB-mass spectra were collected on a JMS-700 double focusing mass spectrometer (JEOL, Tokyo, Japan) with a resolution of 3000 for low resolution and 8000 for high resolution (5% valley definition). For FAB-mass spectra, the source accelerating voltage was operated at 10 kV with a Xe gun, using 3-nitrobenzyl alcohol as the matrix. MALDI-mass spectra were collected on a Voyager DE-PRO (Applied Biosystem, Houston, USA) equipped with a nitrogen laser (337 nm) and operated in the delayed extraction reflector mode. Elemental analyses were performed on a Perkin–Elmer 2400 CHN analyzer. Cyclic voltammetry experiments were performed with a BHI-621B electrochemical analyzer. All measurements were carried out at room temperature with a conventional three-electrode configuration consisting of a platinum working electrode, an auxiliary electrode, and a nonaqueous $Ag/AgNO_3$ reference electrode. The $E_{1/2}$ values were determined as $1/2(E_p^a + E_p^c)$, where E_p^a and E_p^c are the anodic and cathodic peak potentials, respectively. The solvent used was CH_2Cl_2 and the supporting electrolyte was 0.1 M tetrabutylammonium hexafluorophosphate. Electronic absorption spectra were obtained on a Cary 50 Probe UV–visible spectrometer. Emission spectra were recorded in deoxygenated solutions at 298 K by a JASCO FP-6500 fluorescence spectrometer. The emission spectra were collected on samples with o.d. ~0.1 at the excitation wavelength. UV–visible spectra were checked before and after irradiation to monitor any possible sample degradation. Emission maxima were reproducible within 2 nm. Luminescence quantum yields (Φ_{em}) were calculated relative to **Ir(ppy)$_3$** (Φ_{em} = 0.40 in toluene) [19]. Luminescence quantum yields were taken as the average of three separate determinations and were reproducible within 10%. Luminescence lifetimes were determined on an Edinburgh FL920 time-correlated pulsed single-photon-counting instrument. Samples were degassed via freeze–thaw–pump cycle at least three times prior to measurements. Samples were excited at 337 nm from a nitrogen pulsed flashlamp with 1 ns FWHM pulse duration transmitted through a Czerny-Turner design monochromator. Emission was detected at 90° via a second Czerny-Turner design monochromator onto a thermoelectrically cooled red-sensitive photomultipler tube. The resulting photon counts were stored on a microprocessor-based multichannel analyzer. The instrument response function was profiled using a scatter solution and subsequently deconvoluted from the emission data to yield an undisturbed decay. Nonlinear least square fittings of the decay curves were performed with the Levenburg–Marquardt algorithm and implemented by the Edinburgh Instruments F900 software. The reported values represent the average of at least three readings.

2.2. Light-emitting devices fabrication

A layer of 70 nm thick poly(ethylenedioxythiophene):poly(styrene-sulfonic acid) (PEDOT:PSS) (Baytron PVP CH 8000) films was spin-coated on pre-cleaned ITO-coated glass substrates as the hole injection layer and then baked at 100 °C in air for 1 h. Next, the film of CBP containing iridium dendrimer or the neat iridium film (thickness at ~45 nm for **16** and **18**, ~70 nm for **17** and **19**, respectively) as the emitter was spin-coated using dichloroethane as the solvent (concentration: 10 mg mL^{-1} for the host and × wt% Ir dendrimer as the guest) at a spin rate of 2800 rpm (revolution per min.). Then, a electron-transporting and hole blocking 1,3,5-tris(*N*-phenylbenzimidazol-2-yl)benzene (TPBI) film of 40 nm thick was vacuum deposited in a vacuum chamber less than 2.5×10^{-5} torr. Finally, the device was completed by thermal deposition of a LiF/Al (1 nm/120 nm) cathode.

2.3. Hole-only devices fabrication

The hole-only devices in this study consists of a 20 wt% of **16** (or **17**–**19**) in CBP blend thin film sandwiched between transparent indium tin oxide (ITO) anode and metal cathode. Before device fabrication, the ITO glasses (1.5×1.5 cm^2) were ultrasonically cleaned in detergent, de-ionized water, acetone and isopropyl alcohol before the deposition. After routine solvent cleaning, the substrates were treated with UV ozone for 15 min. Then a modified ITO surface was obtained by spin-coating a layer of poly(ethylene dioxythiophene): polystyrenesulfonate

(PEDOT:PSS) (~30 nm). After baking at 130 °C for 1 h, the substrates were then transferred into a nitrogen-filled glove box. The active layer was spin coated (spin rate = 2800 rpm; spin time = 45 s) on top of PEDOT:PSS and then dried in covered glass Petri dishes. The film thickness of the active layer was measured to be 55, 50, 50 and 50 nm, for **16**, **17**, **18** and **19**, respectively. Subsequently, a 20 and 100 nm thick of MoO_3 and aluminum was thermally evaporated under vacuum at a pressure below 6×10^{-6} torr thorough a shadow mask. The active area of the device was 0.12 cm^2.

3. Materials

Chemicals and solvents were reagent grades and purchased from Aldrich, Acros, TCI, and Lancaster Chemical Co. Solvents were dried by standard procedures. All reactions and manipulations were carried out under N_2 with the use of standard inert atmosphere and Schlenk techniques. Solvents were dried by standard procedures. All column chromatography was performed by using silica gel (230–400 mesh, Macherey-Nagel GmbH & Co.) as the stationary phase in a column which is 25–35 cm in length and 2.5 cm in diameter.

3.1. 9,9-Dihexyl-9H-fluorene-2-carbaldehyde (*1*)

2-Bromo-9,9-dihexyl-9*H*-fluorene (20.2 g, 48.9 mmol) was dissolved in 100 mL of dry THF and the solution was cooled to −78 °C. *n*-Butyl lithium in hexane (1.6 M, 30.5 mL, 48.9 mmol) was added dropwise over a period of 30 min. The mixture was allowed to warm to −20 °C in the next 1 h, and 3.8 mL of dry DMF was added. The mixture was stirred at room temperature for 12 h. The reaction was quenched with water and the solution was extracted with diethyl ether. The combined organic extracts were washed with brine solution, dried over $MgSO_4$, and evaporated to dryness. The residue was purified by column chromatography using a mixture of CH_2Cl_2 and hexanes (1:1) as the eluent to afford a white solid (13.4 g, 75%). ^{1}H NMR ($CDCl_3$, 400 MHz, ppm): δ 10.04 (s, 1H, CHO), 7.85 (s, 1H), 7.83–7.80 (m, 2H), 7.76–7.74 (m, 1H), 7.37–7.33 (m, 3H), 2.00–1.97 (m, 4H, CH_2), 1.07–0.97 (m, 12H, CH_2), 0.75 (t, J = 7.2 Hz, 6H, CH_3), 0.56–0.53 (m, 4 H, CH_2).

3.2. 4-(9,9-Dihexyl-9H-fluoren-2-yl)benzaldehyde (*2*)

4-Bromobenzaldehyde (9.25 g, 50 mmol), 9,9-dihexyl-9*H*-fluoren-2-yl-boronic acid (22.5 g, 1.2 equiv.), Na_2CO_3 (12.0 g, 2 equiv.), and $Pd(OAc)_2$ (112 mg, 0.01 equiv.) were dissolved in a mixture of 30 mL of acetone and 35 mL of water. The mixture was stirred at room temperature for 16 h. The reaction was then quenched by pouring the solution into water and the desired compound was extracted with diethyl ether. The collected organic extracts were collected, dried over anhydrous $MgSO_4$. Filtration and removal of the solvent provided a white solid. It was purified by column chromatography using a mixture of dichloromethane and hexanes (1:1) as the eluent to give a yellow oil in 73% yield (16.0 g). ^{1}H NMR ($CDCl_3$, 400 MHz, ppm): δ 10.06 (s, 1H, CHO), 7.97 (d, J = 8.4 Hz, 2H, C_6H_4), 7.82 (d, J = 8.4 Hz, 2H, C_6H_4), 7.78 (d, J = 8.0 Hz, 1H, fluorene), 7.75–7.73 (m, 1H, fluorene), 7.62–7.60 (m, 2H, fluorene), 7.38–7.30 (m, 3H, fluorene), 2.04–1.99 (m, 4H, CH_2), 1.12–1.04 (m, 12H, CH_2), 0.75 (t, J = 7.2 Hz, 6H, CH_3), 0.68–0.66 (m, 4H, CH_2).

3.3. (9,9-Dihexyl-9H-fluoren-2-yl)methanol (*3*)

Compound **1** was dissolved in 40 mL of THF and 40 mL of methanol. Sodium borohydride (2 equiv.) was added slowly to the above solutions in portions, and the solution was allowed to stir for 24 h. The reaction was quenched by pouring the solution into water and the desired compound was extracted with diethyl ether. The organic extracts were collected and dried over anhydrous $MgSO_4$. Filtration and removal of the solvent provided a white solid. It was purified by column chromatography using a mixture of dichloromethane and hexanes (1:1) as the eluent to afford a white powder in 75% yield. ^{1}H NMR ($CDCl_3$, 400 MHz, ppm): δ 7.67–7.64 (m, 2H), 7.32–7.25 (m, 5H), 4.75 (s, 2H, OCH_2), 1.96–1.91 (m, 4H, CH_2), 1.11–1.00 (m, 12H, CH_2), 0.75 (t, J = 7.2 Hz, 6H, CH_3), 0.61–0.55 (m, 4H, CH_2).

3.4. 4-(9,9-Dihexyl-9H-fluoren-2-yl)phenyl)methanol (*4*)

Compound **4** was synthesized by the same procedure as illustrated for compound **3** except that compound **1** was used instead of compound **2**. The compound was isolated as a white solid in 75% yield. ^{1}H NMR ($CDCl_3$, 400 MHz, ppm): δ 7.77–7.73 (m, 2H, fluorene), 7.69 (d, J = 8.4 Hz, 2H, C_6H_4), 7.59–7.57 (m, 2H), 7.48 (d, J = 8.4 Hz, 2H, C_6H_4), 7.39–7.31 (m, 3H, fluorene), 4.74 (d, J = 2.0 Hz, 2H, OCH_2) 1.99–1.96 (m, 4H, CH_2), 1.09–1.01 (m, 12H, CH_2), 0.73 (t, J = 7.2 Hz, 6H, CH_3), 0.66–0.64 (m, 4H, CH_2).

3.5. 2-(Bromomethyl)-9,9-dihexyl-9H-fluorene (*5*)

A mixture of compound **3** (1.82 g, 5.0 mmol) and triphenylphosphine (1.1 equiv.) was dissolved in THF (15 mL) and cooled to 15 °C. *N*-bromosuccinimide (1.1 equiv.) was added all at once. The reaction was stirred for additional 10 min and immediately quenched by cold water. The solids formed were extracted into dichloromethane. The organic extracts were collected, washed with brine, and dried over anhydrous $MgSO_4$. After filtration and removal of the solvent, the crude product was further purified by column chromatography on a silica gel column using a mixture of CH_2Cl_2 and hexanes (1:5 by volume) as the eluent to afford the pure compound as a white solid in 85% yield. ^{1}H NMR ($CDCl_3$, 400 MHz, ppm): δ 7.67–7.61 (m, 2H, fluorene), 7.36–7.30 (m, 5H, fluorene), 4.59 (s, 2H, CH_2Br), 1.98–1.90 (m, 4H, CH_2), 1.12–1.05 (m, 12H, CH_2), 0.75 (t, J = 7.2 Hz, 6H, CH_3), 0.59–0.50 (m, 4H, CH_2).

3.6. 2-(4-(Bromomethyl)phenyl)-9,9-dihexyl-9H- fluorene (*6*)

Compound **6** was synthesized by the same procedure as illustrated for compound **5** except that compound **3** was used instead of compound **4.** The product was isolated as

a white solid in 76% yield. ^{1}H NMR ($CDCl_3$, 400 MHz, ppm): δ 7.73 (d, J = 8.0 Hz, 1H, fluorene), 7.70 (d, J = 7.2 Hz, 1H, fluorene), 7.62 (d, J = 8.4 Hz, 2H, C_6H_4), 7.54 (dd, J = 8.0 Hz and 1.6 Hz, 1H, fluorene), 7.51 (d, J = 1.2 Hz, 1H, fluorene), 7.47 (d, J = 8.4 Hz, 2H, C_6H_4), 7.34–7.28 (m, 3H, fluorene), 4.55 (s, 2H, CH_2Br), 1.99–1.96 (m, 4H, CH_2), 1.09–1.01 (m, 12H, CH_2), 0.73 (t, J = 7.2 Hz, 6H, CH_3), 0.66–0.64 (m, 4H, CH_2).

3.7. (3,5-Bis((9,9-dihexyl-9H-fluoren-2-yl)methoxy)phenyl)-methanol (**7**)

A mixture of 3,5-dihydroxybenzyl alcohol (2.80 g, 20 mmol), potassium carbonate (6.67 g, 40 mmol), compound **5** (2.1 equiv.), and 18-crown-6-ether (0.52 g, 0.2 mmol) in acetone (30 mL) was heated to reflux for 48 h. After being cooled, water was added and the solution was extracted with dicholormethane. The organic extracts were collected, washed with brine, and dried over anhydrous $MgSO_4$. After filtration and removal of the solvent, the crude product was further purified by column chromatography using a mixture of CH_2Cl_2 and hexanes (1:1 by volume) as the eluent. The product was isolated as a white solid in 70% yield. ^{1}H NMR ($CDCl_3$, 400 MHz, ppm): δ 7.67 (d, J = 8.0 Hz, 4H, fluorene), 7.37–7.28 (m, 10H, fluorene), 6.64 (d, J = 2.0 Hz, 2H, C_6H_3), 6.62 (t, J = 2.0 Hz, 1H, C_6H_3), 5.10 (s, 4H, OCH_2), 4.62 (s, 2H, OCH_2), 1.95–1.91 (m, 8H, CH_2), 1.12–0.97 (m, 24H, CH_2), 0.74 (t, J = 7.2 Hz, 12H, CH_3), 0.64–0.56 (m, 8H, CH_2).

3.8. (3,5-Bis(4-(9,9-dihexyl-9H-fluoren-2-yl)benzyloxy)-phenyl)methanol (**8**)

Compound **8** was synthesized by the same procedure as illustrated for compound **7** except that **5** was used instead of **6**. The product was isolated as a white solid in 70% yield. ^{1}H NMR ($CDCl_3$, 400 MHz, ppm): δ 7.74–7.68 (m, 4H, fluorene), 7.67 (d, J = 8.4 Hz, 4H, C_6H_4), 7.56–7.49 (m, 4H, fluorene), 7.47 (d, J = 8.4 Hz, 4H, C_6H_4), 7.33–7.25 (m, 6H, fluorene), 6.67 (d, J = 2.0 Hz, 2H, C_6H_3), 6.60 (t, J = 2.0 Hz, 1H, C_6H_3), 5.07 (s, 4H, OCH_2), 4.61 (s, 2H, OCH_2), 1.95–1.91 (m, 8H, CH_2), 1.12–0.97 (m, 24H, CH_2), 0.74 (t, J = 7.2 Hz, 12H, CH_3), 0.64–0.56 (m, 8H, CH_2).

3.9. Compound **9**

Compound **9** was synthesized by the same procedure as illustrated for compound **5** except that compound **3** was used instead of compound **7**. The product was isolated as a white solid in 70% yield. ^{1}H NMR ($CDCl_3$, 400 MHz, ppm): δ 7.68 (d, J = 8.4 Hz, 4H, fluorene), 7.41–7.25 (m, 10H, fluorene), 6.66 (d, J = 2.0 Hz, 2H, C_6H_3), 6.62 (t, J = 2.0 Hz, 1H, C_6H_3), 5.09 (s, 4H, OCH_2), 4.39 (s, 2H, OCH_2), 1.95–1.91 (m, 8H, CH_2), 1.09–1.00 (m, 24H, CH_2), 0.74 (t, J = 7.2 Hz, 12H, CH_3), 0.56–0.53 (m, 8H, CH_2).

3.10. Compound **10**

Compound **10** was synthesized by the same procedure as illustrated for compound **5** except that compound **3** was used instead of compound **8**. The product was isolated as a white solid in 72% yield. ^{1}H NMR ($CDCl_3$, 400 MHz, ppm): δ 7.74–7.69 (m, 4H, fluorene), 7.67 (d, J = 8.4 Hz, 4H, C_6H_4), 7.56–7.54 (m, 4H, fluorene), 7.51 (d, J = 8.4 Hz, 4H, C_6H_4), 7.34–7.26 (m, 6H, fluorene), 6.67 (d, J = 2.0 Hz, 2H, C_6H_3), 6.61 (t, J = 2.0 Hz, 1H, C_6H_3), 5.09 (s, 4H, OCH_2), 4.43 (s, 2H, OCH_2), 1.99–1.95 (m, 8H, CH_2), 1.11–1.03 (m, 24H, CH_2), 0.73 (t, J = 7.2 Hz, 12H, CH_3), 0.67–0.63 (m, 8H, CH_2).

3.11. 4-(1-Phenyl-1H-benzo[d]imidazol-2-yl)phenol (**11**)

N-Phenyl-*o*-phenylenediamine (9.21 g, 50 mmol), and 4-hydroxybenzaldehyde (6.10 g, 50 mmol) were dissolved in 40 mL of 2-methoxyethanol. The mixture was heated to reflux for 48 h. After cooling, the deposited solids were filtered, washed with dichloromethane, and dried under vacuum to give the desired product (5.1 g, 35%). ^{1}H NMR (DMSO-d_6, 400 MHz, ppm): δ 7.71 (d, J = 7.6 Hz, 1H), 7.57–7.51 (m, 3H), 7.36 (d, 7.6 Hz, 2H), 7.32 (d, J = 8.4 Hz, 2H), 7.26 (t, J = 7.2 Hz, 1H), 7.20 (t, 7.2 Hz, 1H), 7.11 (d, J = 8.0 Hz, 1H), 6.68 (d, 8.4 Hz, 2H). FABMS: m/z 287.2 $(M+H)^+$. Anal. Calcd for $C_{19}H_{14}N_2O$: C, 79.70; H, 4.93; N, 9.78. Found: C, 79.29; H, 5.04; N, 9.58.

Ligands **12**, **13**, **14**, and **15** were synthesized by similar procedures, as described below for compound **12**. Compound **11** (0.73 g, 2.5 mmol), K_2CO_3 (0.35 g, 2.5 mmol), and compound **5** (1.06 g, 2.5 mmol) were dissolved in 30 mL of DMF. The mixture was heated at 100 °C for 24 h. After cooling, the reaction was quenched with water and the mixture was extracted with dicholormethane. The organic extracts were collected, washed with brine, and dried over anhydrous $MgSO_4$. After filtration and removal of the solvent, the crude product was further purified by column chromatography using a mixture of CH_2Cl_2 and hexanes (3:1 by volume) as the eluent to provide **12** as a white solid in 73% yield. ^{1}H NMR ($CDCl_3$, 400 MHz, ppm): δ 7.84 (d, J = 8.0 Hz, 1H), 7.67 (d, J = 8.4 Hz, 2H, C_6H_4), 7.55–7.43 (m, 5H), 7.35–7.27 (m, 8H), 7.20 (d, J = 8.0 Hz, 2H), 6.92 (d, J = 8.4 Hz, 2H, C_6H_4), 5.10 (s, 2H, OCH_2), 1.94–1.90 (m, 4H, CH_2), 1.10–1.00 (m, 12H, CH_2), 0.74 (t, J = 7.2 Hz, 6H, CH_3), 0.60–0.58 (m, 4H, CH_2). FABMS: m/z 633.3 $(M+H)^+$. Anal. Calcd for $C_{45}H_{48}N_2O$: C, 85.40; H, 7.64; N, 4.43. Found: C, 85.24; H, 7.79; N, 4.35.

13: White solid. Yield = 75%. ^{1}H NMR ($CDCl_3$, 400 MHz, ppm): δ 8.14 (d, J = 8.0 Hz, 1H), 7.68–7.60 (m, 8H), 7.54–7.46 (m, 3H), 7.38–7.18 (m, 13H), 6.89 (d, J = 8.4 Hz, 2H), 6.67 (d, J = 2.0 Hz, 2H, C_6H_3), 6.62 (t, J = 2.0 Hz, 1H, C_6H_3), 5.09 (s, 4H, OCH_2), 4.99 (s, 2H, OCH_2), 1.94–1.86 (m, 8H, CH_2), 1.09–0.99 (m, 24H, CH_2), 0.73 (t, J = 7.2 Hz, 12H, CH_3), 0.65–0.54 (m, 8H, CH_2). FABMS: m/z 1101.9 $(M+H)^+$. Anal. Calcd for $C_{78}H_{88}N_2O_3$: C, 85.05; H, 8.05; N, 2.54. Found: C, 85.15; H, 8.22; N, 2.60.

14: White solid. Yield = 56%. ^{1}H NMR ($CDCl_3$, 400 MHz, ppm): δ 7.84 (d, J = 8.0 Hz, 1H), 7.72 (d, J = 8.0 Hz, 1H), 7.69 (d, J = 7.2 Hz, 1H), 7.65 (d, J = 8.0 Hz, 2H), 7.55–7.45 (m, 9H), 7.31–7.28 (m, 6H), 7.22–7.18 (m, 2H), 6.91 (d, J = 8.8 Hz, 2H), 5.09 (s, 2H, OCH_2), 1.99–1.96 (m, 4H, CH_2), 1.09–1.01 (m, 12H, CH_2), 0.73 (t, J = 6.8 Hz, 6H, CH_3), 0.66–0.64 (m, 4H, CH_2). FAB MS: m/z 709.5 $(M+H)^+$. Anal. Calcd for $C_{51}H_{52}N_2O$: C, 86.40; H, 7.39; N, 3.95. Found: C, 86.54; H, 7.40; N, 3.67.

15: White solid. Yield = 56%. ^{1}H NMR ($CDCl_3$, 400 MHz, ppm): δ 8.02 (d, J = 8.0 Hz, 1H), 7.71–7.61 (m, 10H), 7.55–7.47 (m, 12H), 7.34–7.27 (m, 9H), 7.20 (d, J = 8.4 Hz, 1H), 6.92 (d, J = 8.4 Hz, 2H), 6.67 (d, J = 2.0 Hz, 2H, C_6H_3), 6.62 (t, J = 2.0 Hz, 1H, C_6H_3), 5.11 (s, 4H, OCH_2), 4.43 (s, 2H, OCH_2), 1.99–1.96 (m, 8H, CH_2), 1.09–1.01 (m, 24H, CH_2),

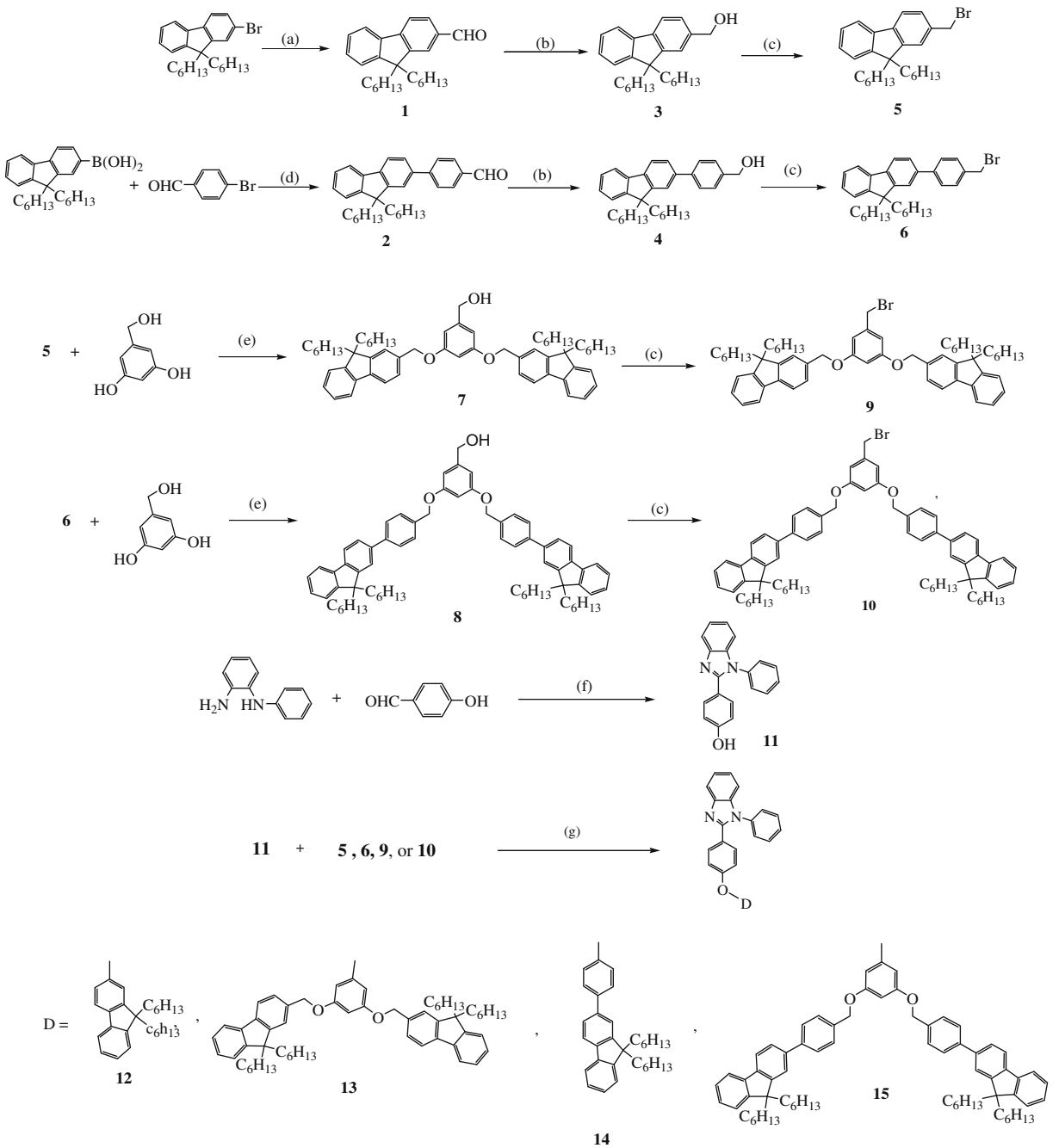

(a) (i) BuLi, THF, -78 °C, (ii) DMF (iii) H^+; (b) $NaBH_4$, THF: MeOH= 1: 1, rt, 16h; (c) NBS, PPh_3, THF, rt, 20 min; (d) $Pd(OAc)_2$, acetone, 35 °C, 16 h; (e) K_2CO_3, 18-crown-6-ether, acetone, reflux, 24h; (f) 2-methoxyethanol, reflux, 16 h; (g) K_2CO_3, DMF, 100 °C, 16 h.

Scheme 1. Synthesis of the dendritic ligands.

0.73 (t, J = 7.2 Hz, 12H, CH_3), 0.66–0.64 (m, 8H, CH_2). FAB-MS: m/z 1253.8 $(M+H)^+$. Anal. Calcd for $C_{90}H_{96}N_2O_3$: C, 86.22; H, 7.72; N, 2.23. Found: C, 85.88; H, 7.58; N, 2.00.

Tris-Ir complexes **16**, **17**, **18**, **19** were synthesized by similar procedures, as described below for **16**. To a flask containing $IrCl_3 \cdot 3H_2O$ (176 mg, 0.50 mmol) and **12** (1.10 g, 1.0 mmol) was added a 3:1 mixture of 2-ethoxyethanol and water (25 mL). The mixture was refluxed for 48 h. After cooling, the reaction was quenched by water, and the mixture was filtered and washed with diethyl

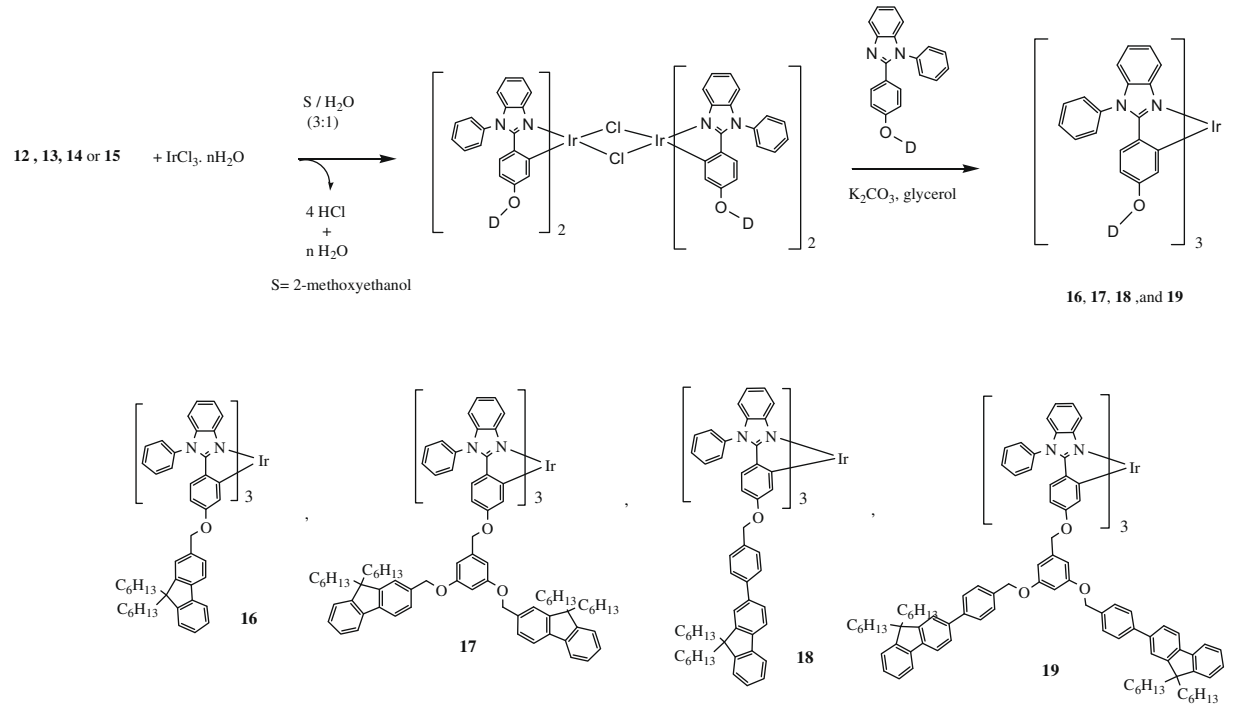

Scheme 2. Synthesis of dendritic iridium complexes.

Table 1
Physical data of the compounds.

cpd	λ_{abs} (log ε), [a] (nm)	λ_{em},(Φ_p)in solution nm (%)	λ_{em}, [c](Φ_p) film nm (%)	τ,[d] μs	τ_r,[e] μs	E_{ox}[f](ΔE_p). mV	E_g[g], eV	HOMO[h], eV	LUMO[i], eV
12	275 (4.63), 307 (4.73)	354[a]				1580	3.64	6.11	2.47
13	273 (4.82), 306 (4.67)	355[a]				1520	3.64	6.05	2.41
14	308 (4.69)	356[a]				1420	3.64	5.95	2.31
15	282 (4.90), 314 (4.70)	357[a]				1420	3.64	5.95	2.31
(G0)$_3$Ir[j]	298 (4.6), 313 (4.6), 375 (4.1), 410 (3.8), 453 (3.5)	517 (45)	534 (15)	1.07	2.37	370 (76)	2.90	4.95	2.0
16	268 (4.66), 308 (4.69), 374 (3.96), 407 (3.74), 432 (3.57)	512[b] (55)	529 (16)	1.46	1.78	394 (63)	2.90	4.92	2.0
17	271 (4.87), 306 (4.64), 366 (3.88), 427 (3.34)	512[b] (63)	525 (30)	1.46	2.31	397 (76)	2.90	4.92	2.0
18	292 (4.60), 317 (4.69), 356 (3.99), 420 (3.34)	513[b] (65)	522 (17)	1.05	1.78	413 (93)	2.90	4.94	2.0
19	296 (4.83), 312 (4.77), 354 (3.77), 407 (3.07)	519[b] (74)	523 (33)	1.02	1.37	414 (124)	2.90	4.94	2.0

[a] Measured in CH_2Cl_2 at 298 K at a concentration of 10^{-5} M. ε is the absorption coefficient.
[b] Recorded in toluene solutions at 298 K. Excitation wavelength was 410 nm for all compounds. Quantum yield was measured in toluene relative to *fac*-Ir(ppy)$_3$ (Φ_p = 0.40).
[c] Neat-film data measured at 298 K. PL quantum efficiencies in films were measured in an integrating sphere.
[d] Measured in toluene solutions at 298 K.
[e] $\tau_r = \tau/\Phi_p$.
[f] Oxidation potential reported is adjusted to the potential of ferrocene ($E_{1/2}$ = 270 mV vs. $Ag/AgNO_3$) which was used as an internal reference. Conditions of cyclic voltammetric measurements: platinum working electrode; $Ag/AgNO_3$ reference electrode. Scan rate: 100 mV/s. Electrolyte: tetrabutylammonium hexafluorophosphate.
[g] E_g: bandgap. E_g was obtained from the absorption spectra.
[h] HOMO level were calculated from CV potentials using ferrocene as a standard [HOMO = 4.8 + ($E_{ox} - E_{Fc}$)].
[i] LUMO derived via equation, E_g = HOMO − LUMO.
[j] Ref. [7].

ether to give μ-chloro-bridged Ir(III) dimer. One equiv. of μ-chloro-bridged Ir(III) dimer was mixed with 2.5 equiv. of K_2CO_3, 2.0 equiv. of **12**, and glycerol (5.0 mL) in a flask. The mixture was heated at 190 °C for 24 h. After cooling, the reaction was quenched with water and the mixture was extracted with dicholormethane. The combined extracts were then washed with brine, dried over $MgSO_4$, filtered, and dried under vacuum. The crude product was isolated by column chromatography using a mixture of CH_2Cl_2 and *n*-hexane (1:1 by volume) as the eluent.

16: Yellow solid. Yield = 56%. ^{1}H NMR ($CDCl_3$, 400 MHz, ppm): δ 7.57–7.45 (m, 21H), 7.28–7.24 (m, 12H), 7.18 (d, J = 8.0 Hz, 3H), 7.06–7.02 (m, 6H), 6.81 (t, J = 6.4 Hz, 3H), 6.72 (s, 3H), 6.60 (d, J = 8.4 Hz, 3H), 6.39 (d, J = 8.0 Hz. 3H), 6.21 (d, J = 8.4 Hz, 3H), 4.87 (d, J = 12.0 Hz, 3H, OCH_2), 4.79 (d, J = 12.0 Hz, 3H, OCH_2), 1.90–1.86 (m, 12H, CH_2), 1.04–0.97 (m, 36H, CH_2), 0.74 (t, J = 7.2 Hz, 18H, CH_3), 0.60–0.56 (m, 12H, CH_2). MADLI-TOF: *m/z* 2087.5 $(M+H)^+$. Anal. Calcd for $C_{135}H_{141}N_6O_3Ir$: C, 86.22; H, 7.72; N, 2.23. Found: C, 85.97; H, 7.42; N, 2.20.

17: Yellow solid. Yield = 15%. ^{1}H NMR ($CDCl_3$, 400 MHz, ppm): δ 7.63–7.56 (m, 18H), 7.52 (t, J = 7.5 Hz, 9H), 7.41 (d, J = 8.0 Hz, 3H), 7.30–7.26 (m, 30H), 7.00–6.94 (m, 6H), 6.79 (t, J = 7.2 Hz, 3H), 6.57–6.54 (m, 12H), 6.30 (s, 3H), 6.04 (s, 3H), 4.95 (s,12H, OCH_2), 4.74 (d, J = 12.0 Hz, 3H, OCH_2), 4.68 (d, J = 12.0 Hz, 3H, OCH_2), 1.92–1.88 (m, 24H, CH_2), 1.06–0.97 (m, 72H, CH_2), 0.71–0.67 (m, 36H, CH_3), 0.58–0.53 (m, 24H, CH_2). MADLI-TOF: *m/z* 3494.8 $(M+H)^+$. Anal. Calcd for $C_{234}H_{261}N_6O_9Ir$: C, 80.44; H, 7.53; N, 2.41. Found: C, 80.21; H, 7.33; N, 2.25.

18: Yellow solid. Yield = 40%. ^{1}H NMR ($CDCl_3$, 400 MHz, ppm): δ 7.67–7.63 (m, 6H), 7.52–7.46 (m, 12H), 7.41 (d, J = 7.6 Hz, 3H), 7.40–7.32 (m, 9H), 7.32–7.28 (m, 9H), 7.24–7.22 (m, 9H), 7.00 (t, J = 7.6 Hz, 3H), 6.92 (d, J = 7.6 Hz, 3H), 6.75 (t, J = 7.6 Hz, 3H), 6.66 (d, J = 2.4 Hz, 3H), 6.53 (d, J = 8.4 Hz, 3H), 6.28 (d, J = 8.4 Hz, 3H), 6.22 (dd, J = 8.4 and 2.4 Hz, 3H), 4.77 (d, J = 12.0 Hz, 3H, OCH_2), 4.74 (d, J = 12.0 Hz, 3H, OCH_2), 1.88–1.80 (m, 12H, CH_2), 1.10–1.02 (m, 36H, CH_2), 0.72 (t, J = 7.2 Hz, 18H, CH_3), 0.66–0.63 (m, 12H, CH_2). MADLI-TOF: *m/z* 2316.4 $(M+H)^+$. Anal. Calcd for $C_{153}H_{153}N_6O_3Ir$: C, 79.34; H, 6.66; N, 3.63. Found: C, 78.97; H, 6.33; N, 3.35.

19: Yellow solid. Yield = 10%. ^{1}H NMR ($CDCl_3$, 400 MHz, ppm): δ 7.74–7.69 (m, 12H), 7.65–7.60 (m, 12H), 7.57–7.50 (m, 21H), 7.45–7.42 (m, 15H), 7.36–7.28 (m, 21H), 6.98–6.92 (m, 6H), 6.88–6.83 (m, 3H), 6.71–6.64 (m, 6H), 6.54–6.45 (m, 15H), 4.95 (s,12H, OCH_2), 4.74 (d, J = 12.0 Hz, 3H, OCH_2), 4.68 (d, J = 12.0 Hz, 3H, OCH_2), 1.92–1.88 (m, 24H, CH_2), 1.06–0.97 (m, 72H, CH_2), 0.71–0.67 (m, 36H, CH_3), 0.58–0.53 (m, 24H, CH_2). MADLI-TOF: *m/z* 3951.3 $(M+H)^+$. Anal. Calcd for $C_{270}H_{285}N_6O_9Ir$: C, 82.09; H, 7.27; N, 2.13. Found: C, 81.71; H, 7.23; N, 2.25.

4. Results and discussion

4.1. Syntheses

Bouveault's synthesis [20] and palladium-catalyzed Suzuki reaction [21] were used to prepare two aldehydes, 9,9-dihexyl-9*H*-fluorene-2-carbaldehyde (**1**), and 4-(9,9-dihexyl-9*H*-fluoren-2-yl)benzaldehyde (**2**) (Scheme 1). Reduction of **1** and **2** with $NaBH_4$ gave the benzyl alcohol **3** and **4** in ~80% yield, which was then treated with *N*-bromosuccinimide and triphenylphosphine to form the benzyl bromides, **5** and **6** [4]. Reaction of compound **5** (or **6**) with 3,5-dihydroxybenzyl alcohol provides compound **7** (or **8**) containing two fluorene branches. Similar to the synthesis

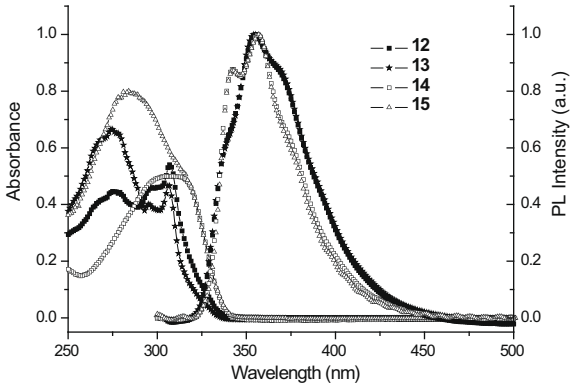

Fig. 1. The absorption spectra and PL of **12**–**15** in CH_2Cl_2 solution.

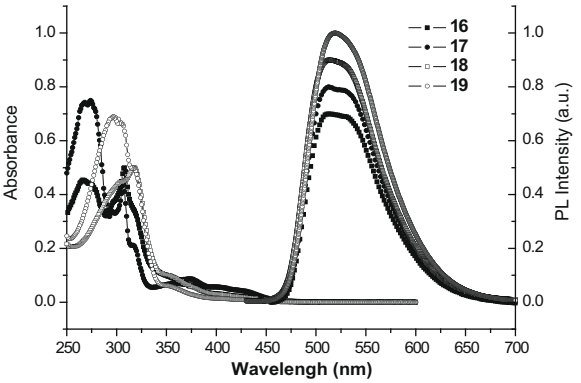

Fig. 2. The absorption spectra of **16**–**19** measured in CH_2Cl_2 solution and the normalized PL spectra of **16**–**19** measured in toluene.

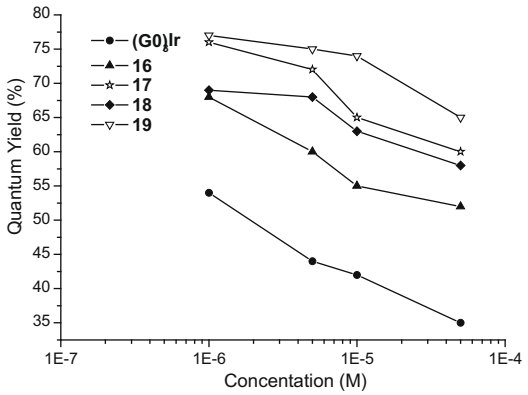

Fig. 3. The variation of quantum yields for **(G0)$_3$Ir**, and **16**–**19** in different concentration in toluene.

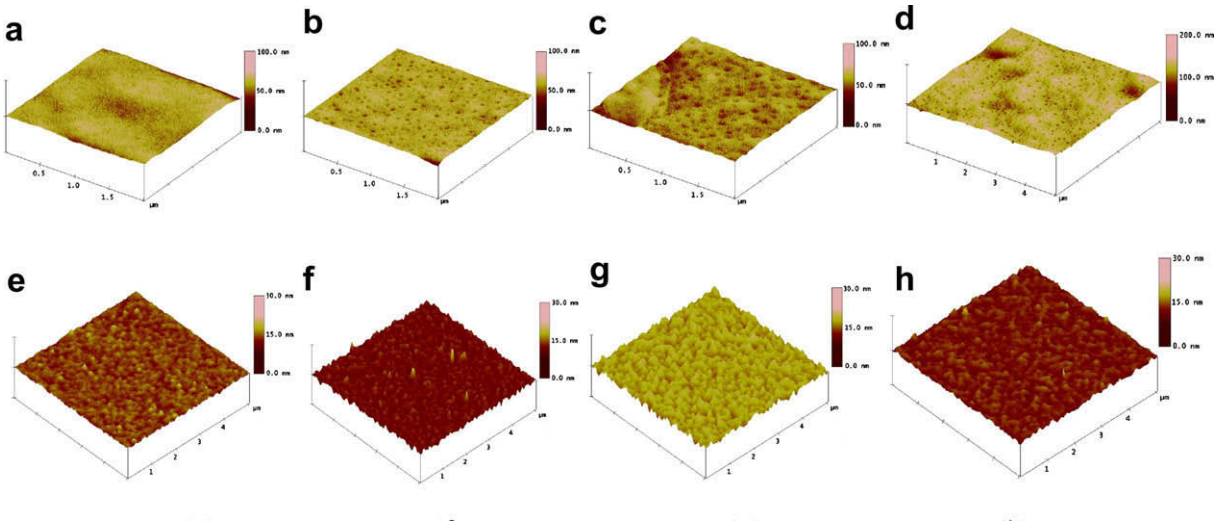

Fig. 4. AFM images from spin-casting films: blend film of CBP: 20 wt% **16** (a); **17** (b); **18** (c); **19** (d) and neat film of **16** (e); **17** (f); **18** (g); **19** (h).

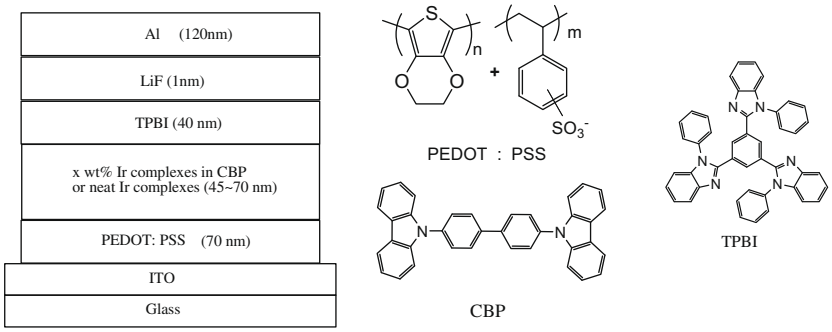

Fig. 5. The configuration of EL devices and the molecular structures of the compounds used.

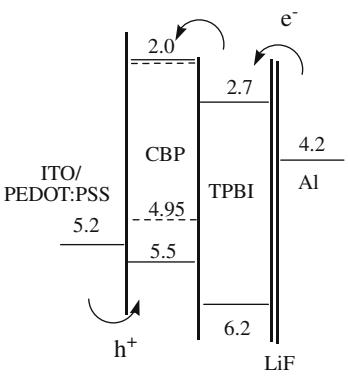

Fig. 6. Relative energy levels of the compounds utilized in DLEDs.

of **5** from **3**, compounds **7** and **8** can be converted to **9** and **10**, respectively. Compound **11**, prepared from *N*-phenyl-*o*-phenylenediamine and 4-hydroxybenzaldehyde, was then allowed to react with **5**, **6**, **9**, and **10**, respectively, using Williamson ether synthesis to form dendritic benzoimidazole ligands **12–15** in 30–90% yields. The preparation of tris-cyclometalated iridium complexes **16–19** involved a two-step synthesis (see Scheme 2): (1) reaction of $IrCl_3 \cdot 3H_2O$ with dendritic ligands **12–15** to from a chloro-bridged dimer intermediate; (2) reaction of the dimer with additional 12–**15** in glycerol at 190 °C. Only the facial (*fac*) isomer was isolated for **16–19**, as evidenced from the NMR spectra.

4.2. Optical properties

The photophysical data of compounds **12–19** are summarized in Table 1. The absorption spectra and photoluminescence (PL) spectra of compounds **12–15** and **16–19** are shown in Figs. 1 and 2, respectively. Absorption bands at ~310 nm ($\varepsilon \sim 10^4$–$10^5\ M^{-1}\ cm^{-1}$) are π–π^* transition characteristic of the benzoimidazolyl moiety, and those at ~275 nm ($\varepsilon \sim 10^4$–$10^5\ M^{-1}\ cm^{-1}$) can be attributed to π–π^* the transition of the peripheral fluorene. Besides the π–π^* transition bands of the ligands, the dendritic iridium complexes **16–19** also exhibit weak absorption bands in the range of ~350–450 nm due to metal-to-ligand charge transfer transitions, ^{1}MLCT and ^{3}MLCT.

The dendritic ligands **12–15** emit in the violet-purple region ($\lambda_{em} \sim 355$ nm) in CH_2Cl_2. Because of non-conjugated nature between the iridium center and the dendron, all dendritic iridium complexes emit green light both in toluene solution and neat film state (λ_{em} = 510–529 nm), similar to their non-dendronized congener, **(G0)$_3$Ir** [7]. The solution PL quantum yields (0.55–0.74 in toluene) of **16–19** compared favorably with that (0.45 in toluene) of the non-dendronized congener, **(G0)$_3$Ir** [7], indicating that the encapsulation indeed more effectively suppresses triplet–triplet annihilation of the emitting core. The phosphorescent lifetimes (1.02–1.46 μs) of these complexes fall into the range of prototype non-dendronized tris-cyclometalated iridium complexes [19]. Apparently, the incorporation of flexible alkyl group or ether linkage does not lead to facile non-radiative decay pathways. The encapsulation efficiency increases as the surface group becomes bulkier (i.e., Φ_{PL} (**18**) > Φ_{PL} (**16**) and Φ_{PL} (**19**) > Φ_{PL} (**17**)), or the generation of the dendron increases (i.e., Φ_{PL} (**17**) > Φ_{PL} (**16**) and Φ_{PL} (**19**) > Φ_{PL} (**18**)). Similar to the quantum yields of the solutions, the trend retains in the film state. The studies of concentration quenching on **16–19** and non-encapsulated complex **(G0)$_3$Ir** further witness the merit of encapsulation from the dendron, that is, the solution quantum yield of **(G0)$_3$Ir** decreases more rapidly than **16–19** as the concentration increases from 10^{-6} M to 5×10^{-4} M (see Fig 3). Compared to the solution state in Table 1, there is a significant drop of PL quantum yields in the solid film state (Φ_{PL} = 0.15–0.33). This is consistent with concentration quenching observed in the toluene solution (*vide supra*). Similar behavior was also reported in other phosphorescent dendrimers [5]. No emission from the peripheral fluorene was noticed, indicating that energy transfer from the peripheral fluorene to the iridium center may occur, or there exists inner filter effect. We found that excitation at the ^{1}MLCT band (~410 nm) of **17** in the film state led to phosphorescent emission of higher intensity by 2.0−2.5 times compared to excitation at the peripheral fluorene (250–300 nm). Therefore, the energy transfer from the dendron to the iridium center is not likely to be the main cause of the increased quantum yields in the larger dendrimers. This is in contrast to FIrpic (iridium(III) bis[(4,6-difluorophenyl)pyridinato-*N*,$C^{2'}$]-3-hydroxypicolinate) derivatives with *N*,*N*'-dicarbazolyl-3,5-benzene-based dendrons [22], which were described to have efficient singlet−singlet and triplet−triplet energy transfer from the dendron to the iridium center.

4.3. Film morphology

Good thin film quality is prerequisite for good performance of OLEDs. Therefore, AFM was used to examine the morphology of the spin-casting films for these complexes. All compounds can be fabricated as good-quality films by spin-coating technique. Fig. 4 shows the AFM images of the spin-coating films (45–70 nm thick), obtained from iridium complexes **16–19**, on plasma treated indium tin oxide (ITO) substrates. The root mean square (RMS) surface roughness of neat film in **16–19** was found to be 0.489, 1.055, 1.287, and 0.667 nm, respectively. The blend films of CBP with 20 wt% of **16–19** had slightly larger RMS surface roughness at 1.175, 0.741, 2.264, and 3.121 nm, respectively.

Table 2
EL data of DLEDs with different composition in the emitting layer.

Emitting-layer	V_{ON}, V	max. L (at V), cd/m^2	max. η_{ext}, %	max. η_c, cd/A	max.η_p, lm/W	J = 20 mA/cm^2; J = 100 mA/cm^2				$\lambda_{em,max}$ (fwhm), nm	CIE, *x*,*y*
						L (at V) cd/m^2	η_{ext}, %	η_c, cd/A	η_p, lm/W		
Blend film											
20 wt% **16** (4.65 mmol)	4.0	14005 (16.0)	9.8	33.8	21.2	3534 (11.6); 10,954 (14.4)	5.7; 3.2	19.5; 11.2	5.3; 2.4	516 (74)	0.29, 0.62
20 wt% **17** (2.77 mmol)	5.0	16229 (16.0)	13.6	45.8	20.6	6926 (8.7); 15,711 (12.5)	10.4; 4.7	35.1; 15.7	12.7; 3.9	514 (72)	0.27, 0.61
40 wt% **17** (5.54 mmol)	5.5	6321 (20.0)	9.4	33.0	9.4	3766 (16.2); –	5.2; –	18.4; –	3.5; –	520 (76)	0.30, 0.62
20 wt% **18** (4.20 mmol)	5.0	19217 (20.0)	8.28	27.9	13.48	3395 (12.5); 10,396 (18.1)	5.04; 3.10	17.0; 10.5	5.1; 2.4	520 (74)	0.31, 0.61
20 wt% **19** (2.45 mmol)	6.0	13,876 (18.0)	9.0	31.1	15.0	4025 (11.5); 10,830 (14.8)	5.8; 3.2	15.0; 20.1	5.5; 2.3	514 (72)	0.28, 0.62
40 wt% **19** (4.91 mmol)	8.0	5814 (20.0)	8.6	26.5	7.6	3073 (15.8); –	5.0; –	31.1; –	3.1; –	514 (72)	0.28, 0.61
Neat film											
16	3.0	4895 (10.0)	3.6	11.4	10.3	1735 (6.0); 4375 (8.6)	2.7; 1.4	8.7; 4.4	4.5; 1.6	516 (76)	0.30, 0.58
17	3.0	993 (10.5)	7.1	23.1	14.5	990 (10.3); 502 (16.9)	1.5; 0.15	5.0; 0.5	1.5; 0.1	516 (74)	0.30, 0.60
18	3.0	5711 (11.5)	4.6	13.7	12.3	1964 (5.8); 4340 (8.2)	3.3;1.5	10.0; 4.4	5.5;1.7	516 (76)	0.30, 0.57
19	5.0	1235 (13.5)	5.0	16.6	9.5	1013 (10.2); 1081 (15.8)	1.5; 0.33	5.1; 1.1	1.6; 0.22	512 (70)	0.26, 0.60

V_{on}, turn-on voltage, at a brightness of 1 cd/m^2; L, luminance; V, voltage; η_{ext}, external quantum efficiency; η_c, current efficiency; η_p, power efficiency; fwhm, full width at half-maximum, max., maximum.

4.4. Electrochemical studies

The electrochemical properties of the ligands (**12**–**15**) and the complexes (**16**–**19**) were studied by cyclic voltammetric (CV) method, and the electrochemical data are summarized in Table 1. All ligands show an irreversible oxidation wave with an onset potential at 1.42–1.58 V vs. $Ag/AgNO_3$, which is characteristic of the peripheral fluorene group. Besides the irreversible oxidation wave of the ligands, a quasi-reversible one-electron oxidation wave attributed to the oxidation of the iridium(III) was detected in the range of ~0.39–0.41 mV vs. $Ag/AgNO_3$. The negligible influence of the dendrons on the oxidation potential of the iridium center is likely due to non-conjugated nature of the spacer between the dendron and the iridium center. No reduction waves up to -2.0 V were detected in these iridium dendrimers. The HOMO (highest occupied molecular orbital) energy levels of compounds **12**–**19** were calculated from cyclic voltammogram in comparison with ferrocene (4.8 eV) [23]. The thus obtained HOMO levels, (~6.0 eV for **12**–**15** and ~4.95 eV for **16**–**19**) in combination with the optical bandgaps which were derived from the optical edges of absorption spectra, were used to calculate the LUMO (lowest unoccupied molecular orbital) energy levels [24]. Both HOMO and LUMO data are collected in Table 1.

4.5. Electroluminescent properties

Electroluminescent (EL) devices of bilayered configuration, ITO/PEDOT:PSS/neat **16**–**19** or *x* wt% of dopant **16**–**19** in CBP (45–70 nm)/TPBI (40 nm)/LiF (1 nm)/Al (120 nm), were fabricated via spin-coating technology (see Fig. 5). Spin-coating technology was used for device fabrication except for the vacuum deposition of TPBI (the electron-transporting and hole-blocking layer). The LED devices without the use of TPBI will not be discussed because the efficiency dropped at least two orders in both cases. The energy band structures of the devices are shown in Fig. 6, and the performance data are presented in Table 2. The EL spectra are shown in Fig. 7. All devices emitted green light and the EL spectra were superimposed with the PL spectra. The absence of emission from CBP suggests that either energy transfer from CBP to the complexes is complete or the trapping of electrons and holes by the complexes is efficient.

Although neat films of good quality can be obtained by spin-coating technique (*vide supra*), the devices using the neat films of the complexes have efficiencies far from ideal: the maximum external quantum efficiencies are lower than 7.1%. The following four factors are probably responsible for the low device efficiencies: (1) T–T annihi-

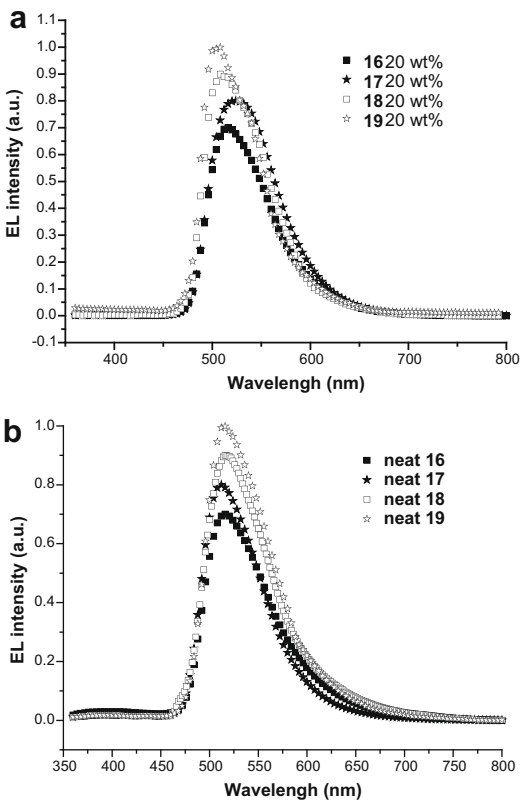

Fig. 7. EL spectra at a driving voltage of 12 V of DLEDs containing (a) **16**–**19** doped with CBP, (b) **16**–**19** neat film.

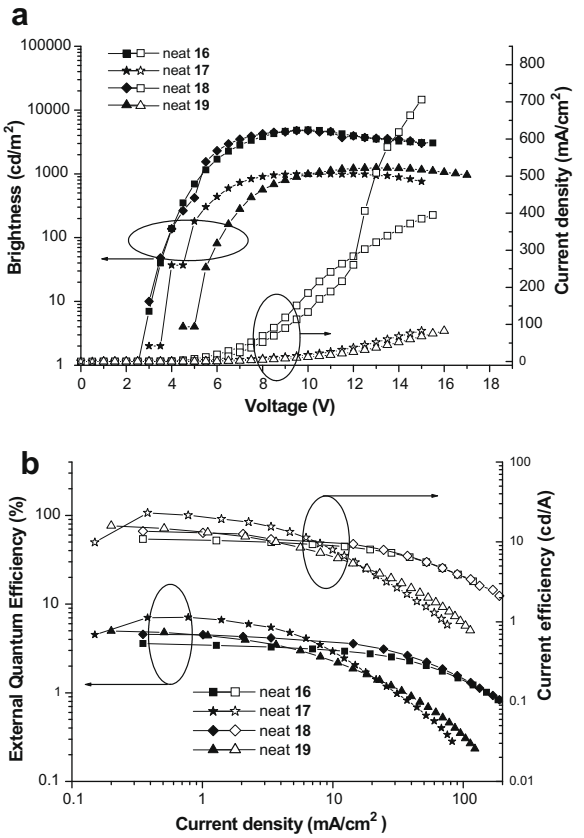

Fig. 8. The electro-optical characteristic of DLEDs containing neat **16**–**19** (a) brightness and current density as a function of voltage, and (b) current efficiency and EQE as a function of current density.

lation due to the high concentration of the guest; (2) the large energy gap between PEDOT:PSS and the HOMO level of peripheral fluorenyl group which hampers the hole injection into the emitting layer; (3) inefficient carrier mobility of the dendrons; (4) quenching of phosphorescence via energy transfer from the iridium center to the dendron due to small gap ($\sim$1000 cm^{-1}) between the triplet energies of the two. Foe example, **15** E_T (77 K, toluene) = 2.55 eV; **10**, E_T (77 K, toluene) = 2.53 eV; **16**, E_T (77 K, toluene) = 2.34 eV. The current–voltage–brightness (*I–V–L*) characteristic and the EQEs and current efficiency vs. current density for the devices based on neat films of **16**–**19** are shown in Fig. 8. DLEDs based on **17** and **19** exhibit much lower current density and brightness. Our observations are consistent with previous report illustrating that the carrier mobility decreases as the dendrimer generation increases [9]. The *I–V–L* characteristic and the EQEs and current efficiency vs. current density of DLEDs containing CBP doped with complexes **16**–**19** are shown in Fig. 9. Among them, the best efficiencies were found to be $\eta_{ext,max}$ = 9.8%, 13.6%, 8.3%, and 9.0%, and $\eta_{c,max}$ = 33.8, 45.8, 27.9, and 31.1 cd/A for the devices with 4.65, 2.77, 4.20, and 2.45 mol% of **16**, **17**, **18**, and **19**, respectively. The significant drop of device efficiencies at dopant concentrations above 40% for all the complexes is likely due to T–T annihilation. The best device performance was achieved at a lower dopant concentrations (mol%) for the devices based on the second-generation dendrimers (**17** and **19**) compared to the devices based on the first-generation dendrimers (**16** and **18**), which may be attributed to the inefficient carrier conductivity of the fluorene-containing dendrons. Inefficient carrier conductivity of the dendron is evident from the *I–V* plots (Fig. 10) of **16** (first generation dendrimer) and **19** (second generation dendrimer) at different doping concentrations: the current decreases as the doping concentration increases at the same driving voltage. Though the current density of **18**-based device was higher than that of **19**-based device, **16**- and **17**-based devices were found to have comparable current density, where the conductivity might be affected by the film morphology. Nevertheless, the efficiency of the device increases as the generation of the dendrimer increases, i.e., **17** > **16** and **19** > **18**. Arylamine-based dendrimers with stilbene dendrons were also reported to have better device efficiency and inferior carrier mobility as the generation increases [9]. It was suggested that the increased spacing of hopping sites in the bulkier dendrimers inhibited transport of majority charge carriers and resulted in a reduction of the mobility. The influence of the dendron on the device efficiency may also be accounted by the same token in our

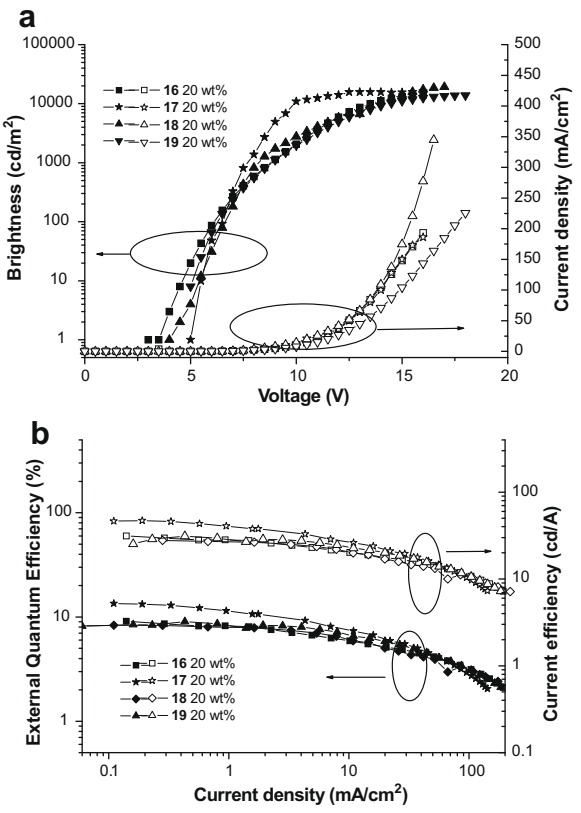

Fig. 9. The electro-optical characteristic of DLEDs containing *x* wt% **16**–**19** in CBP: (a) brightness and current density as a function of voltage; (b) current efficiency and EQE as a function of current density.

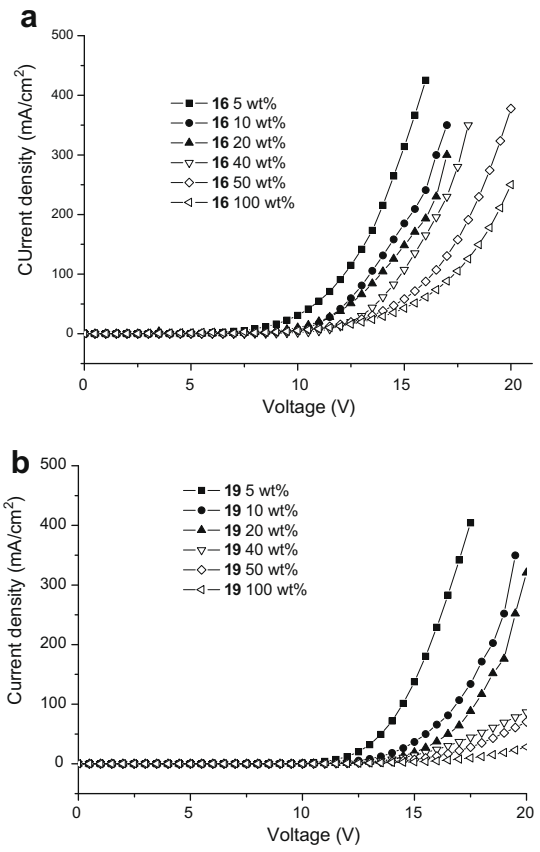

Fig. 10. The electro-optical characteristic of current–voltage (*I–V*) curves in DLEDs containing CBP with various dopant ratios of (a) compound **16** and (b) compound **19**.

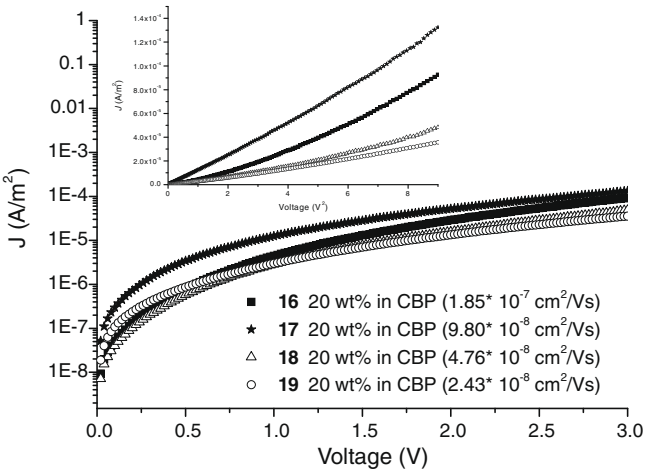

Fig. 11. The current–voltage (J–V) plots of hole-only devices with 20 wt% of **16**–**19** in CBP. Insert is the log$J$–V^2 curves.

case. It is interesting to note that neat film devices also behave similarly (see Fig. 11).

4.6. Hole mobility properties

Space-charge-limited current (SCLC) flow technique was used to measure the mobility of charge carriers in the films [25]. In spite of the ambipolar carrier-transporting characteristic of CBP [26], no discernible currents were detected for the blend film of CBP with the compounds synthesized in electron-only devices, indicating that the electron mobility was negligible in the film. This is consistent with the poor performance of DLEDs without the presence of TPBI (*vide supra*). In comparison, from the hole-only devices the hole mobilities can be determined precisely by fitting the dark current vs. voltage (J–V) curves for single carrier devices to SCLC model [27–28]. The dark current is given by $J = 9\varepsilon_0\varepsilon_r\mu V^2/8L^3$ [29], where $\varepsilon_0\varepsilon_r$ is the permittivity of the dendrimer, μ is the carrier mobility, and L is the device thickness. From the capacitance–voltage measurements we have obtained a relative dielectric constant ε_r of 0.65, 1.81, 1.30, 1.98 for the blend film of 20 wt% of **16**, **17**, **18**, and **19** in CBP, respectively. Therefore, the hole mobilities were calculated to be 1.85×10^{-7}, 9.80×10^{-8}, 4.76×10^{-8}, and 2.43×10^{-8} cm^2/Vs for the blend films of **16**, **17**, **18** and **19**, respectively. These observations are consistent with the lower current density measured for DLEDs based on larger dendrimers, i.e., device of **17** < device **16** and device **19** < device **18** (*vide supra*). The lower hole mobility of the larger dendrimers (**17** and **19**) is likely due to increased spacing of hopping sites [9]. The better efficiencies of the devices for the larger dendrimers may be stemmed from the increased waiting time of charge carriers which will increase the probability of recombination, similar to that reported for triarylamine-cored distyrylbenzene-based dendrimers [9]. The device based on the neat film has a lower efficiency than that based on the CBP blend film, which may also be attributed to the non-conductivity of the former, and the very narrow exciton recombination region near the interface between the neat film and TPBI. Compared with the iridium complexes encapsulated with benzyl ether dendrons we reported earlier [17], the hole mobilities of the dendrimers in this study appear to be ~one order lower. The hole mobilities of the previous dendrimers were measured to be 2.7×10^{-6}, and 9.2×10^{-7} cm^2/V s for the 20 wt% CBP blend films of **(G1)$_3$Ir** (first generation dendrimer) and **(G2)$_3$Ir** (second generation dendrimer), respectively. Possibly the larger fluorene moiety increases spacing of hopping sites and results in a reduction of the mobility (*vide supra*). The somewhat lower device efficiencies in this study may be due to the less balanced hole and electron mobilities (the electron mobility of TPBI is ~10^{-5} cm^2/(V s) [30]).

5. Conclusions

In conclusion, we have synthesized a series of benzoimidazole-based dendritic complexes of iridium dendrimers containing Fréchet-type dendrons with peripheral fluoenyl surface groups. These iridium dendrimers emit green light with high PL quantum yields, and can be spin-cast as films of good quality. The electroluminescent devices fabricated by the spin-coating technique have high-performance of electro-optical properties. One of the devices with the structure of ITO/PEDOT:PSS/CBP: **17** (20 wt%)/TPBI/LiF/Al has a maximum EQE of 13.58% and a maximum current efficiency of 45.7 cd/A. The high HOMO level of the peripheral fluoenyl surface group leads to a larger turn on voltage. EL devices based on the dendrimers of higher generation have a lower current density because of the slower carrier mobility of the higher generation dendrimer. However, EL devices from dendrimers of higher generation exhibit higher EQEs and current efficiencies.

Acknowledgments

We thank the Academia Sinica, National Chiao Tung University and the National Science Council for supporting this work.

References

[1] C.W. Tang, S.A. VanSlyke, Appl. Phys. Lett. 51 (1987) 913.
[2] (a) P.W. Wang, Y.J. Liu, C. Devadoss, P. Bharathi, J.S. Moore, Adv. Mater. 8 (1996) 237;
(b) M. Halim, J.N.G. Pillow, I.D.N. Samuel, P.L. Burn, Adv. Mater. 11 (1999) 371;
(c) A.W. Freeman, S.C. Koene, P.R.L. Malenfant, M.E. Thomson, J.M.J. Fréchet, J. Am. Chem. Soc. 122 (2000) 12385;
(d) A. Adronov, J.M.J. Fréchet, Chem. Commun. (2000) 1701;
(e) J.M. Lupton, I.D.W. Samuel, R. Beavington, M.J. Frampton, P.L. Burn, H. Bässler, Phys. Rev. B 63 (2001) 5206.
[3] (a) H.Z. Xie, M.W. Liu, O.Y. Wang, X.H. Zhang, C.S. Lee, L.S. Hung, S.T. Lee, P.F. Teng, H.L. Kwong, H. Zheng, C. Che, Adv. Mater. 13 (2001) 1245;
(b) J. Ostrowski, M.R. Robinson, A.J. Heeger, G.C. Bazan, Chem. Commun. (2002) 784;
(c) J.-P. Duan, P.-P. Sun, C.-H. Cheng, Adv. Mater. 15 (2003) 224;
(d) Y.-J. Su, H.-L. Huang, C.-L. Li, C.-H. Chien, Y.-T. Tao, P.-T. Chou, S. Datta, R.-S. Liu, Adv. Mater. 15 (2003) 884;
(e) A.B. Tamayo, B.D. Alleyne, P.I. Djurovich, S. Lamansky, I. Tsyba, N.N. Ho, R. Bau, M.E. Thompson, J. Am. Chem. Soc. 125 (2003) 7377;
(f) W. Lu, B.-X. Mi, M.C.W. Chan, Z. Hui, N. Zhu, S.-T. Lee, C.-M. Che, Chem. Commun. (2002) 206;
(g) B.W. D'Andrade, J. Brooks, V. Adamovich, M.E. Thompson, S.R. Forrest, Adv. Mater. 14 (2002) 1032;
(h) Y. Ma, H. Zhang, J. Shen, C.-M. Che, Synth. Met. 94 (1998) 245;
(i) Y. Ma, C.-M. Che, H.-Y. Chao, X. Zhou, W.H. Chan, J. Shen, Adv. Mater. 11 (1999) 852.
[4] (a) M.A. Baldo, D.F. O'Brien, Y. You, A. Shoustikov, S. Sibley, M.E. Thompson, S.R. Forrest, Nature 395 (1998) 151;
(b) M.A. Baldo, D.F. O'Brien, M.E. Thompson, S.R. Forrest, Phys. Rev. B 60 (1999) 14422;
(c) C. Adachi, M.A. Baldo, M.E. Thompson, S.R. Forrest, J. Appl. Phys.. 90 (2001) 5048.
[5] T.D. Anthopoulos, M.J. Frampton, E.B. Namdas, P.L. Burn, I.D.W. Samuel, Adv. Mater. 16 (2004) 557.
[6] S.-C. Lo, N.A.H. Male, J.P.J. Markham, S.W. Magennis, P.L. Burn, I.D.W. Samuel, Adv. Mater. 14 (2002) 975.
[7] J. Ding, J. Gao, Y. Cheng, Z. Xie, L. Wang, D. Ma, X. Jing, F. Wang, Adv. Funct. Mater. 16 (2006) 575.
[8] S.-C. Lo, T.D. Anthopoulos, E.B. Namdas, P.L. Burn, I.D.W. Samuel, Adv. Mater. 17 (2005) 1945.
[9] (a) J.M. Lupton, I.D.W. Samuel, R. Beavington, P.L. Burn, H. Bässler, Adv. Mater. 13 (2001) 258;
(b) J.M. Lupton, I.D.W. Samuel, R. Beavington, M.J. Frampton, P.L. Burn, H. Bässler, Phys. Rev. 63 (2001) 155206.
[10] P.L. Burn, S.-C. Lo, I.D.W. Samuel, Adv. Mater. 19 (2007) 1675.
[11] (a) G. Zhou, W.-Y. Wong, B. Yao, Z. Xie, L. Wang, Angew. Chem., Int. Ed. 46 (2007) 1149;
(b) B. Liang, L. Wang, Y. Xu, H. Shi, Y. Cao, Adv. Funct. Mater. 17 (2007) 3580.
[12] (a) J.P.J. Markham, S.-C. Lo, S.W. Magennis, P.L. Burn, I.D.W. Samuel, Appl. Phys. Lett. 80 (2002) 2645;
(b) R.N. Bera, N. Cumpstey, P.L. Burn, I.D.W. Samuel, Adv. Funct. Mater. 17 (2007) 1149.
[13] S.-C. Lo, G.J. Richard, J.P.J. Markham, E.B. Namdas, S. Sharma, P.L. Burn, I.D.W. Samuel, Adv. Funct. Mater. 15 (2005) 1451.
[14] (a) T.D. Anthopoulos, J.P.J. Markham, E.B. Namdas, J.R. Lawrence, I.D.W. Samuel, S.-C. Lo, P.L. Burn, Org. Electron. 4 (2003) 71;
(b) N. Cumpstey, R.N. Bera, P.L. Burn, I.D.W. Samuel, Macromolecules 38 (2005) 9564.
[15] (a) T. Tsuzuki, N. Shirasawa, T. Suzuki, S. Tokito, Jpn. J. Appl. Phys. 44 (2005) 4151;
(b) S.-C. Lo, E.B. Namdas, C.P. Shipley, J.P.J. Markham, T.D. Anthopolous, P.L. Burn, I.D.W. Samuel, Org. Electron. 7 (2006) 85.
[16] W.-S. Huang, J.T. Lin, C.-H. Chien, Y.-T. Tao, S.-S. Sun, Y.-S. Wen, Chem. Mater. 16 (2004) 2480.
[17] W.-S. Huang, J.T. Lin, H.-C. Lin, Org. Electron. 9 (2008) 557.
[18] (a) C.-C. Wu, T.-L. Liu, W.-Y. Hung, Y.-T. Lin, K.-T. Wong, R.-T. Chen, Y.M. Chen, Y.-Y. Chieh, J. Am. Chem. Soc. 125 (2003) 3710;
(b) C.-C. Wu, Y.-T. Lin, K.-T. Wong, R.-T. Chen, Y.-Y. Chieh, Adv. Mater. 16 (2004) 61;
(c) C.-C. Wu, T.-L. Liu, Y.-T. Lin, W.-Y. Hung, T.-H. Ke, Appl. Phys. Lett. 85 (2004) 1172;
(d) C.-C. Wu, W.-G. Liu, W.-Y. Hung, T.-L. Liu, K.-T. Wong, Y.-Y. Chieh, R.-T. Chen, T.-H. Hung, T.-C. Chao, Y.-M. Chen, Appl. Phys. Lett. 87 (2005) 052103.
[19] A. Tsuboyama, H. Iwawaki, M. Furugori, T. Mukaide, J. Kamatani, S. Igawa, T. Moriyama, S. Miura, T. Takiguchi, S. Okada, M. Hoshino, K. Ueno, J. Am. Chem. Soc. 125 (2003) 12971.
[20] (a) L. Bouveault, Bull. Soc. Chim. Fr. 31 (1994) 1306;
(b) J.D. Einhorn, J. Org. Chem. 49 (1984) 1078;
S.M. Denton, A. Wood, Synlett (1999) 55.
[21] L. Liu, Y. Zhang, B. Xin, J. Org. Chem. 71 (2006) 3994.
[22] T.-H. Kwon, M.K. Kim, J. Kwon, D.-Y. Shin, S.J. Park, C.-L. Lee, J.-J. Kim, J.-I. Hong, Chem. Mater. 19 (2007) 3673.
[23] J. Pommerehne, H. Vestweber, W. Guss, R.F. Mahrt, H. Bässler, M. Porsch, J. Daub, Adv. Mater. 7 (1995) 551.
[24] (a) B.E. Koene, D.E. Loy, M.E. Thompson, Chem. Mater. 10 (1998) 2235;
(b) M. Thelakkat, H.-W. Schmidt, Adv. Mater. 10 (1998) 219.
[25] D. Hertel, H. Bässler, ChemPhysChem 9 (2008) 666.
[26] H. Kanai, S. Ichinosawa, Y. Sato, Syn. Met. 91 (1997) 195.
[27] P.W.M. Blom, M.J.M. De Jong, M.G. Van Munster, Phys. Rev. B 55 (1997) R656.
[28] D.H. Dunlap, P.E. Parris, V.M. Kenkre, Phys. Rev. Lett. 77 (1996) 542.
[29] W.D. Gill, J. Appl. Phys. 43 (1972) 5033.
[30] Y. Li, M.K. Fung, Z. Xie, S.-T. Lee, L.-S. Hung, J. Shi, Adv. Mater. 14 (2002) 1317.